# $Li_{2.5}V_2(PO_4)_3$: A Room-Temperature Analogue to the Fast-Ion Conducting High-Temperature $\gamma$-Phase of $Li_3V_2(PO_4)_3$

S.-C. Yin,[†] P. S. Strobel,[‡] H. Grondey,[§,||] and L. F. Nazar*[,†]

*Department of Chemistry, University of Waterloo, Waterloo, Ontario, Canada N2L 3G1, CNRS Cristallographie, BP166, Grenoble Cedex 9, France, and NMR Facility, Department of Chemistry, University of Toronto, Toronto, Ontario, Canada M5S 1A1*

*Received August 28, 2003. Revised Manuscript Received December 29, 2003*

The structure of the NASICON-like phase $Li_{2.5}V_2(PO_4)_3$ has been determined by X-ray and neutron powder diffraction, demonstrating that it crystallizes in the space group $P2_1/n$ ($a = 8.5539(4)$ Å; $b = 8.6099(4)$ Å; $c = 11.9825(5)$ Å; $\beta = 90.002(7)°$). Combined studies using $^{6,7}$Li MAS NMR, EPR, and ac impedance spectroscopy show that this pseudo-orthorhombic lattice represents a room-temperature analogue of the high-temperature orthorhombic phase $\gamma$-$Li_3Sc_2(PO_4)_3$. Lithium disorder over partially vacant sites leads to enhanced ion mobility. EPR spectroscopy confirms the presence of localized $V^{4+}$ in the lattice, whose short-range order with $V^{3+}$ gives rise to five resolvable Li shifts in the $^{6,7}$Li MAS NMR spectrum. These shifts can be rationalized by consideration of the Fermi-contact interactions arising from the difference between $V^{3+}$ and $V^{4+}$ coupling in the three lithium sites.

## Introduction

Lithium transition metal phosphates are promising candidates as positive electrode materials in Li-ion batteries. Those of interest possess an $M_x(PO_4)_y$ framework that houses interstitial $Li^+$ ions. Extraction of lithium from the lattice—equivalent to charging the cell—is simultaneous with oxidation of the transition metal element in the framework to preserve charge balance. Important is that the reinsertion reaction be highly reversible. Many phosphates are suitable candidates in this respect, although various factors can limit the reversibility including deleterious side reactions. Nonetheless, phosphates usually exhibit excellent stability on long-term cycling by comparison to lithium metal oxides, and essentially no loss of oxygen from the framework or reactivity with the electrolyte.[1] These are all important characteristics for the positive electrode. Some of the best-known phosphates are related to the fast-ion conducting NASICON (sodium silicon ionic conductor). This nonredox active zirconium silicophosphate, once extensively studied as an electrolyte in sodium−sulfur cells, accommodates highly mobile sodium cations in its cavities.[2] Subsequent studies incorporated a redox-active element in the framework; hence, the resultant materials were investigated as electrodes in rechargeable Na cells owing to their mixed ionic/electronic properties.[3] Transport of electrons within the lattice, however, was found to be slow as the materials were very poor electronic conductors.[4]

The sodium transition metal phosphates $Na_3M_2(PO_4)_3$ (M = Ti, V, Cr, and Fe) are isostructural with rhombohedral NASICON;[5] however, there is a monoclinic modification which has a slightly different structure. The two differ in the way that the metal octahedra and phosphate/silicate tetrahedra are linked, and in the location of the alkali sites. The density of the rhombohedral phase is slightly less than that of the monoclinic, implying less mobility of the cations in the pristine phase.[6] However, mobility varies with the nature/number of the sites occupied in the lattice, which can change with lithium extraction or insertion as a result of re-ordering. Hence, the monoclinic lithium vanadium phosphate phase shows better electrochemical properties[7] than the rhombohedral. The experiences a kinetic limitation on *re*-insertion of Li due to structural changes incurred on lithium extraction.[8] The rhombohedral lithium phases are not accessible by direct reaction since the sodium phases are the more thermodynamically stable. They must be prepared by ion exchange.[8,9] Conversely, the monoclinic lithium-containing phases

* To whom correspondence should be addressed. E-mail: lfnazar@uwaterloo.ca.
[†] University of Waterloo.
[‡] CNRS Cristallographie.
[§] University of Toronto.
[||] Deceased.

(1) Manthiram, A.; Goodenough, J. B. *J. Power Sources* **1989**, *26*, 403.
(2) Hong, H. Y-P. *Mater. Res Bull.* **1976**, *11*, 173.
(3) Nanjundaswamy, K. S.; Padhi, A. K.; Goodenough, J. B.; Okada, S.; Ohtsuka, H.; Arai, H.; Yamaki, J. *Solid State Ionics* **1996**, *92*, 1.
(4) Padhi, A. K.; Nanjudaswamy, K. S.; Goodenough, J. B. *J. Electrochem. Soc.* **1997**, *144*, 1188.
(5) Pintard-Screpel, M.; D'Yvoire, F.; Remy, F. C. R. *Acad. Sci.* **1978**, *C286*, 381. Delmas, C.; Olazcuaga, R.; Cherkaoui, F.; Brochu, R.; Le Flem, G. *C. R. Acad. Sci.* **1978**, *C287*, 169. Pintard-Screpel, M.; D'Yvoire, F.; Bretey, E. *Solid State Ionics* **1983**, *9/10*, 851. Gopalakrishnan, J.; Rangan, K. K. *Chem. Mater.* **1992**, *4*, 745.
(6) Goodenough, J. B.; Hong, H. Y.-P.; Kafalas, J. A.. *Mater. Res. Bull.* **1976**, *11*, 203.
(7) Barker, J.; Saidi, M. Y. U.S. Patent 5,871,866, 1999.
(8) Gaubicher, J.; Goward, G.; Wurm, C.; Masquelier, C.; Nazar, L. F. *Chem. Mater.* **2000**, *12*, 3240.
(9) Cushing, B. L.; Goodenough, J. B. *J. Solid State Chem.* **2001**, *162*, 196.

10.1021/cm034802f CCC: $27.50 
Published on Web 03/23/2004

are the most thermodynamically stable and hence can be prepared directly from the elements.

Among these monoclinic $A_3M_2(PO_4)_3$ phases, the first studied in detail were M = Sc and Fe. Single-crystal investigations[10] have been reported, along with reversible lithium insertion into the Fe phase, accompanied by insertion/reduction of the $Fe^{3+}$ to $Fe^{2+}$.[11] The sites for lithium insertion in this lattice, which accommodates up to five lithium ions, were identified by neutron diffraction measurements.[12] Lithium extraction is not possible, owing to the exceptionally high potential $Fe^{3+} \rightarrow Fe^{4+}$ couple, making it less desirable as a Li-ion cathode. Ideally, the positive electrode acts as the reservoir for Li ions in the cell as the anode (carbon) is lithium-free. The most interesting phase, *vis-a-vis* electrochemical storage devices, $Li_3V_2(PO_4)_3$, has been examined only recently. The structure of the room-temperature α-phase was reported first based on powder data[13] and later confirmed by single-crystal investigation.[14] Like the analogous iron phase, the lattice transforms to a $\beta$-phase (monoclinic) at 393 K and to an orthorhombic superionic $\gamma$-phase at 453 K.[15] The first report of the electrochemical properties of the α-phase showed that two Li ions could be reversibly extracted from the lattice.[7] More recently, Saidi et al.[16] and Huang et al.[14] demonstrated that all three Li can be reversibly cycled, leading to a promising reversible capacity close to theoretical (200 mA·h/g). In the latter work, the encapsulation of the phosphate crystallites in a carbon matrix enables this to take place even at relatively fast rates.

In these reports, the rich complexity of the electrochemical curve on oxidation and reduction of $Li_3V_2(PO_4)_3$ has been noted. The nature of the numerous two-phase transitions on oxidation are due to Li re-ordering within an essentially static $V_2(PO_4)_3$ framework, as shown by both accurate first-principles calculations[17] and our neutron/X-ray diffraction studies coupled with solid-state $^7$Li NMR spectroscopy.[18] Remarkably good agreement in the location of the lithium sites was achieved between these two studies. In addition, our experiments revealed the existence of charge ordering on the vanadium sites in the phase formed by extraction of one lithium from $Li_3V^{+3}{}_2(PO_4)_3$. $Li_2V_2(PO_4)_3$ contains columns of ordered $V^{4+}/V^{3+}$, demonstrating that the electrons are pinned on the $V^{3+}$ (on both diffraction and NMR time scales). In fact, vanadium charge ordering is intimately linked to Li site ordering as shown in this study, and in our subsequent report which revealed the nature of the hysteresis between the oxidation and reduction curve.[19]

The electrochemical curve also showed the existence of a phase at $x = 2.5$ midway between the starting phase, $x = 3.0$, and the charge-ordered phase, $x = 2.0$, but its structure was not identified. The very small voltage jump signaled by its formation indicated that it is similar in energy to the phases on either side. Hence, we expect it has a similar structure—but one that is intermediate between the two other phases, with partial occupancy of some sites. The computational study also predicted the existence of this phase, although the authors were unable to identify the exact arrangement of the lithium sites. In this paper, we present a combined neutron/X-ray diffraction, solid-state $^{6,7}$Li MAS NMR/EPR spectroscopic, and ac impedance study that collectively show that this phase is qualitatively similar in nature to the high-temperature superionic $\gamma$-phase of $Li_3Sc_2(PO_4)_3$.

## Experimental Section

**Sample Preparation.** Microcrystalline α-$Li_3V_2(PO_4)_3$ was prepared by mixing stoichiometric amounts of $Li_2CO_3$ (Aldrich, 99.99%), $V_2O_5$ (99.6%), and $NH_4H_2PO_4$ (99.99%). The mixture was heated at 300 °C for 3 h, reground, and fired at 850 °C for 12 h under a flow of 7% $H_2/N_2$. The $^6$Li-enriched sample for the $^6$Li MAS NMR study was prepared using $^6Li_2CO_3$ as the lithium source. Chemical oxidation/reduction methods were used to obtain bulk quantity samples for neutron diffraction measurements. The $x = 2.75$, 2.5, 2.25, and 2.0 compositions were prepared by stoichiometric chemical oxidation of α-$Li_3V_2(PO_4)_3$ with 1 M $NOBF_4$ in acetonitrile for 24 h in an Ar-filled glovebox to reach the desired lithium content. The products in each case were filtered and washed with acetonitrile three times to remove remaining salts. To ensure the materials were of the correct stoichiometry, their open-circuit voltage was measured vs $Li^+/Li$. A short oxidation or reduction step ($\Delta x$ (Li) ~ 0.1) revealed the presence of the desired single-phase composition through examination of the change in slope of the voltage−composition curve. The samples obtained were structurally similar to those obtained electrochemically, as proven by the identical X-ray diffraction patterns recorded for selected samples. The delithiated material $Li_{2.5}V_2(PO_4)_3$ was also subjected to chemical analysis to confirm the Li/V ratio.

**Powder Neutron Diffraction.** About 2 g of $Li_{2.5}V_2(PO_4)_3$ was loaded in a vanadium can in an Ar-filled glovebox. Neutron diffraction was performed on the D2B high-resolution diffractometer at the Institut Laue-Langevin (ILL), Grenoble ($\lambda = 1.5940$ Å). The data set was collected at 300 K for 12 h over the range $2\theta = 10-160°$, using a step size of 0.05°.

**Powder X-ray Diffraction.** Samples were measured on a Siemens D500 powder diffractometer ($\lambda = 1.5406$ Å) in the range $2\theta = 10-100°$ at a count rate of 19 s per step of 0.02°. Le Bail full pattern matching was employed to confirm the space group prior to Rietveld refinement and determine initial unit cell parameters.[20]

**Rietveld Refinement.** The refinement was performed using GSAS software, initially using fractional coordinates from our single-crystal $Li_3V_2(PO_4)_3$ analysis. A Chebyshev

(10) Bykov, A. B.; Chirkin, A. P.; Demyanets, L. N.; Doronin, S. N.; Genkina, E. A.; Ivanov-Shits, A. K.; Kondratyuk, I. P.; Maksimov, B. A.; Mel'Nikov, O. K.; Muradyan, L. N.; Simonov, V. I.; Timofeeva, V. A. *Solid State Ionics* **1990**, *38*, 31. Note that sites $Li_2$ and $Li_3$ in $Li_3V_2(PO_4)_3$ are switched in our study by comparison to this reference.

(11) Masquelier, C.; Padhi, A. K.; Nanjudaswamy, K. S.; Goodenough, J. B. *J. Solid State Chem.* **1998**, *135*, 228. Anderssson, A. S.; Kalska, B.; Eyob, P.; Aernout, D.; Haggstrom, L.; Thomas, J. O. *Solid State Ionics* **2001**, *140*, 63.

(12) Andersson, A. S.; Kalska, B.; Eyob, P.; Aernout, D.; Häggström, L.; Thomas, J. O. *Solid State Ionics* **2001**, *140*, 63. Eyob, P.; Andersson, A. S.; Thomas, J. O. *J. Mater. Chem.*, **2002**, *12*, 2343.

(13) Ohkawa, H.; Yoshida, K.; Saito, M.; Uematsu, K.; Toda, K.; Sato, M. *Chem. Lett.* **1999**, 1017.

(14) Huang, H.; Yin, S.-C.; Kerr, T.; Nazar, L. F. *Adv. Mater.* **2002**, *14* (21), 1525.

(15) Sato, M.; Ohkawa, H.; Yoshida, K.; Saito, M. Uematsu, K. Toda, K. *Solid State Ionics* **2000**, *135*, 137.

(16) Saïdi, M. Y.; Barker, J.; Huang, H.; Adamson, G. *Electrochem. Solid-State Lett.* **2002**, *5*, A149.

(17) Morgan, D.; Ceder, G.; Saidi, Y.; Barker, J.; Swoyer, J.; Huang, H.; Adamson, G. *Chem. Mater.* **2002**, *14*, 4684. Morgan, D.; Ceder, G.; Saidi, M. Y.; Barker, J.; Swoyer, J.; Huang, H.; Adamson, G. *J. Power Sources* **2003**, *119*, 755.

(18) Yin, S. C.; Grondey, H.; Strobel, P.; Huang, H.; Nazar, L. F. *J. Am. Chem. Soc.* **2003**, *125*, 326.

(19) Yin, S. C.; Strobel, P.; Grondey, H.; Anne, M.; Nazar, L. F. *J. Am. Chem. Soc.* **2003**, *125*, 10402.

(20) Le Bail, A.; Duroy, H.; Fourquet, J. L. *Mater. Res. Bull.* **1988**, *23*, 447−452. Cox, D. E. High-resolution powder diffraction and structure determination. In *Synchrotron Radiation Crystallography*; Coppens, P.; Academic Press: New York, 1992; Chapter 9, pp 186−254.

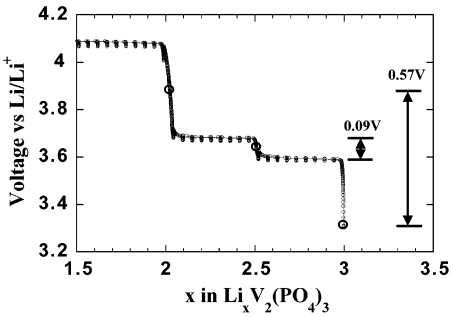


**Figure 1.** Expanded GITT electrochemical curve showing the small step at 3.65 V corresponding to the $Li_{2.5}V_2(PO_4)_3$ phase.

function with 12 coefficients was used to model the background, and a pseudo-Voigt function was used to describe the peak shape. Scale factor, zero point, lattice parameters, atomic positions, and thermal factor were iteratively refined with 87 variables in $Li_{2.5}V_2(PO_4)_3$. The vanadium positions were based on an initial combined X-ray and neutron refinement and kept fixed during the final stages of the neutron refinement. This was necessary owing to the essentially zero neutron scattering length of vanadium. The X-ray data were not included at this stage as the refinement was improved without it. The thermal parameter for vanadium was kept fixed during the refinement and thermal factor constraints were applied to P, O, and Li atoms separately.

**$^{6,7}$Li MAS NMR Measurements.** Samples were hermetically sealed in zirconia rotors fitted with airtight Kel-F caps in an Ar-filled glovebox. The spectra were recorded on a Bruker DSX200 at the resonance frequency of 77.789 MHz for $^7$Li or 29.454 MHz for $^6$Li. $^7$Li-lactate or $^6$Li-carbonate was used as the reference (0 ppm). To acquire the spectra, a single-pulse sequence was used with a 2.5 $\mu$s (90°) pulse length and a repetition time of 2 s. The spinning speeds were varied from 6 to 11.5 kHz to identify the isotropic chemical shifts. The spectral peak area integration was calculated by the DmFit program.[21]

**Electron Paramagnetic Resonance (EPR) Measurements.** Samples were sealed in quartz tubes, and the spectra were recorded on a Bruker EMX EPR spectrometer. The field was varied from 2400 to 4800 G with a resonance frequency of 9.803 GHz.

**ac Impedance Measurements.** Samples were loaded in Swagelok design cells under Ar with nickel rods as the contact electrodes. The cells were subsequently pressed at a pressure of 3 tons, and the pellet thickness was obtained by measuring the difference between the total length of the cell and the nickel rods. Spectra were recorded on an Autolab PGSTAT30 potentiostat with a frequency response analyzer. Frequencies were varied from 10 kHz to 0.01 Hz with 0.1-V amplitude.

**Electrochemistry Measurements.** Electrochemical cells were constructed using a Swagelok design, utilizing 1 M $LiPF_6$/EC-DMC (Merck) as the electrolyte. Cathodes comprised $Li_3V_2(PO_4)_3$ Super S (MMM) and PVDF binder with the weight ratio 80:15:5. Cells were assembled in a glovebox under Ar with $O_2$ and $H_2O$ lower than 5 ppm. Samples were examined in the galvanostatic mode with a current equivalent to a C/10 rate.

## Results and Discussion

**(1) Framework Structure.** *X-ray Diffraction and Electrochemistry.* The features of the electrochemical voltage−composition curve on oxidation (de-insertion) in the region near $Li_{2.5}V_2(PO_4)_3$ are shown in Figure 1 as an expanded region of the full curve. As discussed in previous reports,[19] the plateaus signify a two-phase transition between the single-phase compositions that lie on the voltage steps. The overall jump of 0.6 V between the open-circuit voltage of the starting phase $Li_{3.0}V_2(PO_4)_3$ (LVP3.0) and the single phase after extraction of one lithium ion, $Li_{2.0}V_2(PO_4)_3$ (LVP2.0), is significant: this corresponds to oxidation of one electron to give a mixed oxidation state $V^{3+/4+}$. The electrons are not delocalized over the two vanadium sites as would be desirable for optimum electron transport, but are fully localized on the $V^{3+}$ sites as described previously.[18] Because of the size difference between the two $V^{3+}$ and $V^{4+}$ cations, the vanadium−oxygen octahedra exhibit an ordered structure composed of alternating columns. The monoclinic $P2_1/n$ structure of LVP2.0 is illustrated in Figure 2a for reference, along with that of the starting phase, LVP3.0 (Figure 2c). There is a significant difference between the location of the Li sites between these two phases. The three crystallographically independent Li sites in LVP3.0: Li(1), Li(2), and Li(3) are 4-, 5-, and 5-coordinate, respectively. The lithium that is extracted, Li(3), is the most weakly bound as determined from bond-sum calculations. Its extraction results in a slight re-organization of the lattice and a shift in the location of Li(2) to give it a coordination environment similar to that of Li(1), while Li(1) remains essentially fixed in position. These changes in site energy and partial oxidation of the metal cations give rise to the free-energy difference of the phases, and hence to the observed voltage jump.

The voltage difference between the two plateaus that span the single phase, $Li_{2.5}V_2(PO_4)_3$ (LVP2.5), is smaller however (0.09V), indicating that LVP2.5 represents a small thermodynamic perturbation in the curve. Although the material can be extracted from the electrochemical cell, a sample was isolated (without complications of binder or carbon) by accurate stoichiometric chemical oxidation of LVP3.0. The preparation of large quantities for physical study is enabled by this method. Its X-ray diffraction pattern is shown in Figure 3a. Full-pattern matching (Le Bail fitting) of LVP2.5 was carried out to determine the best space group for this cell, as the $P2_1/n$ monoclinic phases that lie on either side are close to pseudo-orthorhombic ($\beta$ angles of 90.6° and 90.2°). The sample contained an impurity of the second phase, $x = 2.0$, as indicated by the X-ray data and from the NMR spectrum (see below). Its addition to the pattern resulted in an improvement of the fit. The presence of this more oxidized phase is due to a small excess of the oxidizing agent used to prepare $x = 2.5$ from the $x = 3.0$ phase. Control of the stoichiometry of this phase was more difficult than for any of the others, as it sits on a very small voltage step on the electrochemical curve. Thus, even a tiny deviation from stoichiometry can lead to formation of a second phase.[22]

Refinement of the LVP2.5 cell in the $P2_1/n$ space group yielded a $\beta$ angle so close to 90° that we also attempted to refine the cell in an orthorhombic space group (*Pbna*). The agreement factors and goodness-of-fit values between the $P2_1/n$ ($R_{wp} = 6.93\%$; $\chi^2 = 2.15$) and the *Pbna* ($R_{wp} = 7.55\%$; $\chi^2 = 2.55$) space groups were very close. However, the slightly better agreement

(21) Massiot, D.; Fayon, F.; Capron, M.; King, I.; Le Calvé, S.; Alonso, B.; Durand, J.-O.; Bujoli, B.; Gan, Z.; Hoatson, G. *Magn. Reson. Chem.* **2002**, *40*, 70−76.

(22) Multiple synthesis efforts at making LVP2.5 revealed that the fraction of the LVP2.0 contaminant varied from between 26% (as obtained in early studies, and used for the neutron diffraction studies) to as low as 5% (obtained in later NMR studies), this being dependent on the synthesis conditions and sample size.

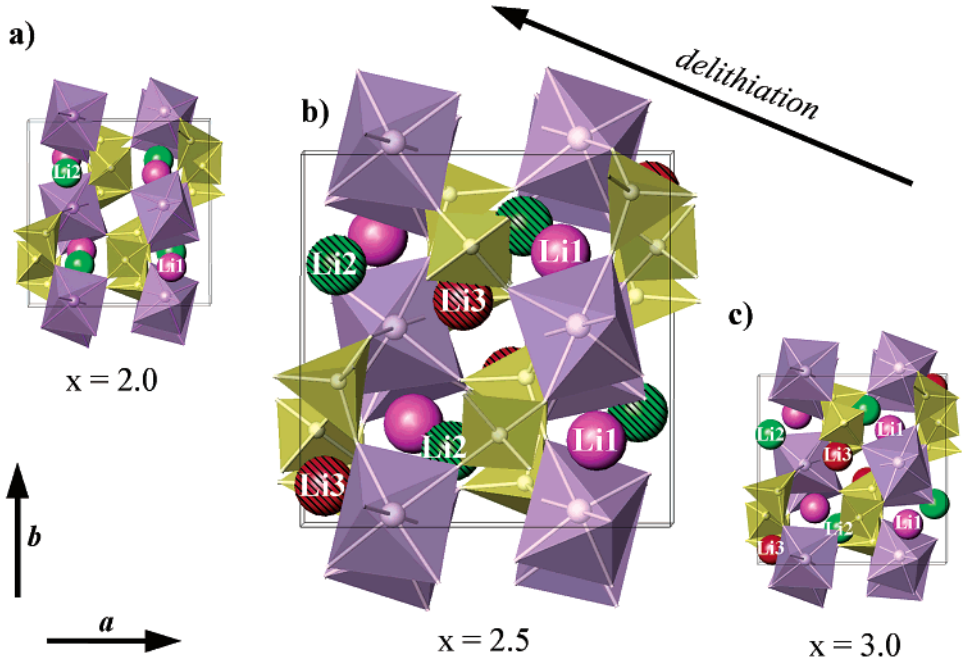


**Figure 2.** Structural variation in $Li_xV_2(PO_4)_3$ on de-insertion from $x = 3 \rightarrow 2$. (a) $x = 2.0$; (b) $x = 2.5$; (c) $x = 3.0$. V−O octahedra (purple) are connected via their apexes with P−O (yellow) tetrahedra to form a 3D framework. Li sites are labeled; the hatched circles for Li(2) and Li(3) indicate partial occupancy.

factors of the $P2_1/n$ cell imply that this is the better unit cell choice. Clearly, the departure from orthorhombic symmetry is very small. The Le Bail refinement of the monoclinic cell gave parameters of $a = 8.5502(3)$ Å, $b = 8.6123(3)$ Å, $c = 11.9983(4)$ Å, and $\beta = 90.146(4)°$.

*Neutron Diffraction*. The neutron diffraction pattern of D-$Li_{2.5}V_2(PO_4)_3$ is shown in Figure 3b. This sample also contained a small impurity of the second phase, $x = 2.0$. Its addition to the pattern resulted in a small improvement of the Le Bail fit to yield good agreement factors ($\chi^2 = 1.75$; $R_{wp} = 2.97\%$). A reasonable structural solution for $Li_{2.5}V_2(PO_4)_3$ was found by Rietveld analysis using interpolated fractional coordinates between $x = 2.0$ and $x = 3.0$ phases as a starting point, in the space group $P2_1/n$. The V(1) and V(2) positions were fixed from XRD refinement, as the neutron scattering length is close to zero. Fourier mapping was employed to locate the lithium sites after refinement of the framework in the absence of lithium. Initially, two sites were readily identified, Li(1) and Li(2), which were similar to the sites in the D3.0 phase. After these were introduced into the structure, and their fractional coordinates were refined, an additional site was located (Li(3)) that was assumed to be partially occupied. As the initial refinement consistently yielded occupancy values for Li(1) at 1.0 (which is reasonable as the site is fully occupied in two phases on either side), the refinement was completed using a constraint where $n(\text{Li}(2) + \text{Li}(3)) = 1.5$. The refinement converged to the values shown in Table 1. As shown in the table, and in Figure 3b, a good agreement was achieved between the experimental and calculated neutron diffraction patterns, with very good reliability factors ($R_{wp} = 5.21\%$; $\chi^2 = 6.00$). The fraction of the $x = 2.0$ phase was refined to 26%. All Li sites (Li(1) fully occupied and Li(2) and Li(3) partially occupied) give satisfactory Li−O bond lengths (Table 2). The refined neutron parameters ($a = 8.5539(4)$ Å, $b = 8.6099(4)$ Å, $c = 11.9825(5)$ Å, and $\beta = 90.002(7)°$) are very close to those of the Le Bail X-ray refinement. We note that the neutron $\beta$ angle is 90° within experimental error, whereas the X-ray value was 90.15°. We ascribe this small discrepancy to the lower resolution of the neutron diffraction experiment.

The $V_2(PO_4)_3$ framework is extremely similar to that in the parent phase, $x = 3.0$. The host lattice is composed of interconnected corner-shared P−O tetrahedra and V−O octahedra, forming a 3D framework shown in Figure 2b. The phosphate tetrahedra have typical average P−O bond lengths of 1.54 Å. The average V(1)−O and V(2)−O bond distances in the slightly distorted vanadium octahedra are 1.969 and 1.998 Å, respectively (Table 2). Thus, V(1)−O is slightly more contracted compared to the starting phase, $Li_3V_2(PO_4)_3$ (2.005 Å), but the change in V(2)−O is negligible. Although the framework is essentially the same as that in the previous phase, the three Li sites account for a halfway situation vis-a-vis the two adjacent members. The site that remains almost fixed in occupancy and position is Li(1), which is also fully occupied in both $x = 3$ and $x = 2$ phases (see next section). The site shifts slightly between these three phases, but the coordination environment remains essentially the same. Li(2), almost fully occupied, also occupies a similar position as in the $x = 3.0$ phase, but is slightly shifted closer to the location of Li(2) in $x = 2.0$. Li(3) has a location similar to that in the $x = 3.0$ phase, but is only half occupied. Constraining the occupation of Li(2) + Li(3) = 1.5 provided the most satisfactory agreement factors, but it is difficult to determine whether the occupancy ratio of Li(2) and Li(3) is 1:0.5 or 0.9:0.6. Using a model with a constraint for Li(2):Li(3) of 1:0.5 did not improve the fit significantly. Allowing the Li($n$) atomic displacement parameters to vary independently led to an even lower occupation of Li(2), and correspondingly lower for Li(1). It is nonetheless clear that D2.5 corresponds to removal of one-half

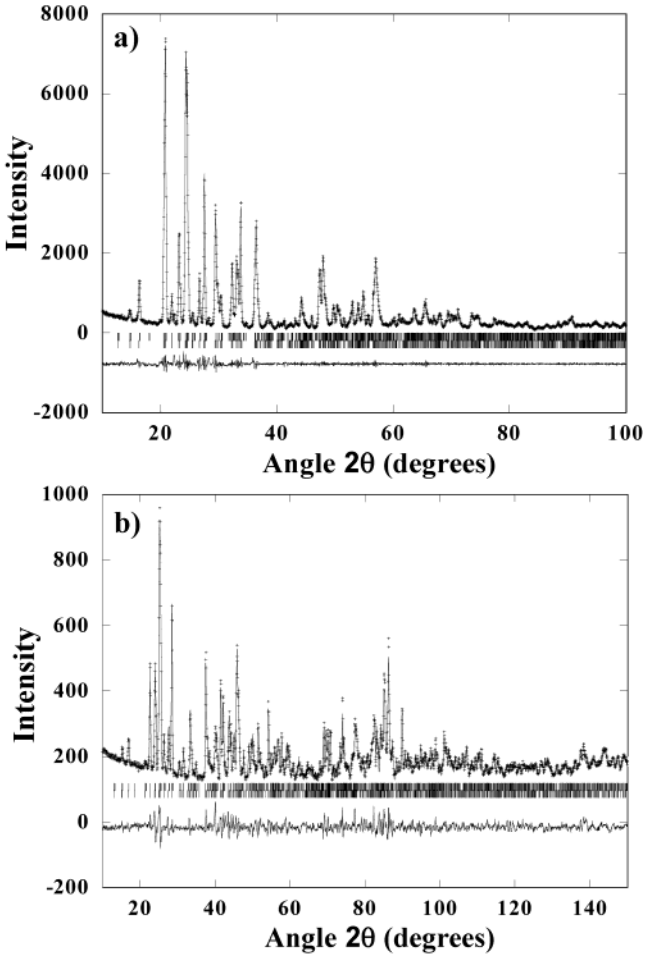


**Figure 3.** (a) X-ray diffraction pattern of $Li_{2.5}V_2(PO_4)_3$ ($\lambda$ = 1.5406 Å) and the full pattern fit; (b) neutron diffraction pattern ($\lambda$ = 1.5940 Å) of $Li_{2.5}V_2(PO_4)_3$ and Rietveld fit. The experimental (+) and calculated (−) data are shown, with *hkl* positions (|) labeled (upper: $Li_{2.0}V_2(PO_4)_3$; lower: $Li_{2.5}V_2(PO_4)_3$), and the difference curve below.

of the lithium from the Li(3) site, with the possible existence of disorder between the Li(2) and Li(3) sites. Recall that the subsequent phase, $x = 2.0$, corresponds to *full* extraction of Li(3), which also results in alteration in the position of Li(2).

*EPR Spectra.* The belief that either short- or long-range charge ordering existed in D2.5, not observable directly in the diffraction study, was raised by the observation of multiple isotropic Li sites in its MAS NMR spectra (see below). These could not be explained by any reasonable occupation of Li within the lattice, although complex Fermi-coupling arising from difference vanadium charge states could account for the multiple shifts. The existence of $V^{3+}$ and $V^{4+}$ in the LVP2.5 phase is shown by EPR measurements on the LVP3.0, 2.5, and 2.0 phases (Figure 4).

We first examined the EPR spectrum of $Li_2V_2(PO_4)_3$, which contains 50% *localized* $V^{4+}$.[18] Characteristic hyperfine features are evident in the spectrum (Figure 4c) that closely resemble those of $VO(H_2O)_5^{2+}$.[23] The latter is a classic $d^1$ paramagnetic ion that has been used as an EPR spin probe because of its characteristic spectrum. As the $3d^1$ ground state has nondegenerate orbitals with no other electronic excited states close in energy, the long spin−lattice relaxation time makes it easy to observe a spectrum at room temperature. The splitting of the lines in the spectra is due to the hyperfine coupling between the vanadium-51 nucleus (spin: $^7/_2$) and the electron spin that gives rise to an eight-line hyperfine pattern. The two sets of overlapping hyperfine components arising from $g||$ and $g\perp$ can be partially resolved in the solid state, as shown for $VO(H_2O)_5$.[23] The EPR spectrum of the $V^{3+/4+}$ charge-ordered phase $Li_2V_2(PO_4)_3$ displays the same features. The latter are superimposed upon a broad spectrum resulting from the combined effects of zero-field splitting and rapid relaxation from the $d^2$ electron state ($V^{3+}$) in the system. This broad feature is present in the spectra of all three samples and dominates the spectrum of $Li_3V_2(PO_4)_3$, which contains 100% $V^{3+}$, as expected (Figure 4a). For $Li_{2.5}V_2(PO_4)_3$, the hyperfine feature is also clearly seen, albeit with a lower magnitude than $Li_2V_2(PO_4)_3$, as expected due to dilution effects (Figure 4b). Although these data do not demonstrate that the $d^1$ electron is localized in $Li_{2.5}V_2(PO_4)_3$ on a time scale longer than that "sensed" by EPR ($\sim 10^{10}$ Hz), they do confirm the existence of the two valence states. The very low electronic conductivity exhibited by $Li_{2.5}V_2(PO_4)_3$ (see last section) furthermore suggests that rapid hopping between the $V^{3+/4+}$ sites does not occur.

If the hyperfine features correspond to long-range charge ordering, a true unit cell with reduced symmetry would be required since the $P2_1/n$ cell contains only two unique vanadium sites. Various symmetry solutions exist. First, there are three possible subgroups of the

**Table 1. Summary of D-Li2.5V2(PO4)3 Refinement (Neutron Data)**

Cell Parameters

S.G.: $P2_1/n$
$a$ = 8.5539(4) Å; $b$ = 8.6099(4) Å; $c$ = 11.9825(5) Å; $\beta$ = 90.002(7)°
$V$ = 882.49 Å$^3$; $Z$ = 4
atomic positions (all in Wyckoff site 4e)

| name | *x* | *y* | *z* | *U**100 | fract |
|---|---|---|---|---|---|
| V(1) | 0.25054 | 0.4606 | 0.12595 | 0.006 | 1.0 |
| V(2) | 0.74918 | 0.46844 | 0.39561 | 0.006 | 1.0 |
| P(1) | 0.1069(17) | 0.1023(18) | 0.1462(14) | 0.0149(16) | 1.0 |
| P(2) | 0.6014(17) | 0.1108(18) | 0.3517(13) | 0.0149(16) | 1.0 |
| P(3) | 0.0390(13) | 0.2537(23) | 0.4955(13) | 0.0149(16) | 1.0 |
| O(1) | 0.9295(16) | 0.1103(20) | 0.1481(15) | 0.0169(6) | 1.0 |
| O(2) | 0.1594(20) | 0.9873(20) | 0.2334(15) | 0.0169(6) | 1.0 |
| O(3) | 0.1702(21) | 0.0565(21) | 0.0349(14) | 0.0169(6) | 1.0 |
| O(4) | 0.1614(19) | 0.2682(20) | 0.1733(14) | 0.0169(6) | 1.0 |
| O(5) | 0.4246(17) | 0.0968(19) | 0.3323(14) | 0.0169(6) | 1.0 |
| O(6) | 0.6880(19) | 0.9908(21) | 0.2796(14) | 0.0169(6) | 1.0 |
| O(7) | 0.6470(20) | 0.0669(21) | 0.4692(13) | 0.0169(6) | 1.0 |
| O(8) | 0.6505(21) | 0.2753(20) | 0.3146(14) | 0.0169(6) | 1.0 |
| O(9) | 0.9424(19) | 0.1407(18) | 0.5648(12) | 0.0169(6) | 1.0 |
| O(10) | 0.9297(19) | 0.3354(17) | 0.4123(13) | 0.0169(6) | 1.0 |
| O(11) | 0.1604(17) | 0.1644(20) | 0.4235(14) | 0.0169(6) | 1.0 |
| O(12) | 0.1254(16) | 0.3465(21) | 0.5828(13) | 0.0169(6) | 1.0 |
| Li(1) | 0.299(6) | 0.270(5) | 0.323(4) | 0.026(7) | 1.0 |
| Li(2) | 0.905(6) | 0.300(6) | 0.203(4) | 0.026(7) | 0.96(6) |
| Li(3) | 0.562(10) | 0.394(10) | 0.187(6) | 0.026(7) | 0.54(6) |

Refinement Parameters

angular range = 10° to 150°; number of variables = 87
constraints: $U_{iso}$(P1) = $U_{iso}$(P2) = $U_{iso}$(P3)
$U_{iso}$(O1) = $U_{iso}$(O2) = ... = $U_{iso}$(O12)
$U_{iso}$(Li1) = $U_{iso}$(Li2) = $U_{iso}$(Li3)
frac(Li2) + frac(Li3) = 1.5
$R_{wp}$ = 5.68%; $\chi^2$= 6.363; $R_{F2}$ = 9.77%

(23) Parish, R. V. In *NMR, NQR, EPR and Mossbauer Spectroscopy in Inorganic Chemistry*; Ellis Horwood Series in Inorganic Chemistry; Burgess, J., Ed.; Ellis Horwood Ltd.: New York, 1990.

**Table 2. Summary of Li−O and V−O Distances (Å) in D-$Li_{2.5}V_2(PO_4)_3$**

| | | | | | | | | | |
|---|---|---|---|---|---|---|---|---|---|
| Li(1)−O(2) | 2.03(5) | Li(2)−O(1) | 1.77(5) | Li(3)−O(12) | 2.47(9) | V(1)−O(2) | 1.867(18) | V(2)−O(1) | 2.025(17) |
| Li(1)−O(4) | 2.15(6) | Li(2)−O(4) | 2.24(5) | Li(3)−O(2) | 2.27(8) | V(1)−O(4) | 1.910(17) | V(2)−O(3) | 1.814(16) |
| Li(1)−O(5) | 1.84(5) | Li(2)−O(6) | 1.84(5) | Li(3)−O(6) | 2.33(9) | V(1)−O(5) | 1.968(16) | V(2)−O(6) | 2.176(17) |
| Li(1)−O(11) | 1.92(5) | Li(2)−O(8) | 2.56(5) | Li(3)−O(8) | 1.99(9) | V(1)−O(7) | 2.090(15) | V(2)−O(8) | 2.102(17) |
| | | Li(2)−O(10) | 2.53(5) | Li(3)−O(9) | 1.81(9) | V(1)−O(9) | 1.997(14) | V(2)−O(10) | 1.933(16) |
| | | | | | | V(1)−O(11) | 2.003(16) | V(2)−O(12) | 1.938(16) |

Bond sum calculation: Li(1): 1.032; Li(2): 1.035; Li(3): 0.949.

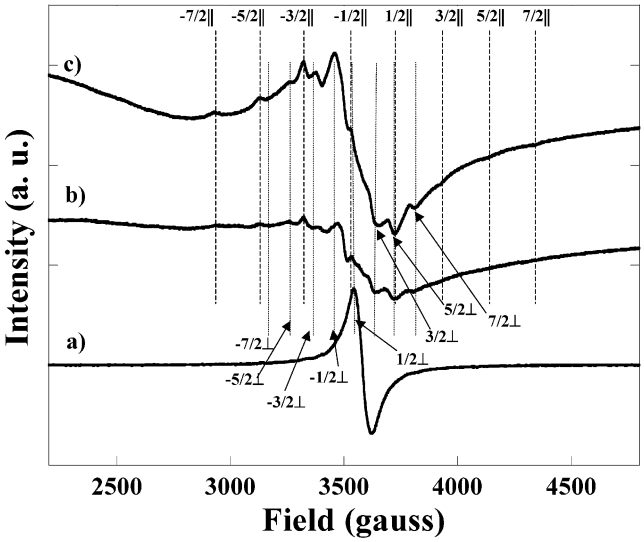


**Figure 4.** EPR spectrum of $Li_xV_2(PO_4)_3$ phases: (a) $x = 3.0$, (b) $x = 2.5$, and (c) $x = 2.0$. For the $x = 2.0$ and 2.5 phases, the positions of the $g||$ and $g\perp$ hyperfine components are labeled according to ref 23.

space group $P2_1/n$ with reduced symmetry on the vanadium sites: $Pc$, $P2_1$, and $P\bar{1}$. Second, within each subgroup, the V(1) and V(2) sites are split into two, to yield four vanadium sites that we will call V(1), V(1s), V(2), and V(2s). In these cells, because V(1) is the site that is oxidized in forming LVP2.0, we assume that either V(1) or V(1s) is oxidized in LVP2.5. The $P\bar{1}$ model shown in Figure 5 demonstrates one possibility of charge ordering in the cell, although clearly other models are possible.

A Le Bail fit of the X-ray pattern to both a $Pc$ and $P2_1$ cell yielded good agreement factors, similar to the $P2_1/n$ cell. However, attempts to carry out a Rietveld refinement of the neutron diffraction data on the structure in any of the very low symmetry $P2_1/n$ subgroups failed to converge satisfactorily, either due to limitations of the data or due to the ordering being short range in nature. Long-range order may be perturbed by the many different ways in which the $V^{4+}$ can be accommodated within the lattice. Irrespective of whether the ordering is long or short range in nature, the model above will further help to explain the origin of NMR shifts in $Li_{2.5}V_2(PO_4)_3$ described in the following section.

*$^{6,7}$Li MAS NMR.* The $^6$Li MAS NMR spectrum of this material exhibits five resolvable peaks at 189, 122, 51, 28, and −9 ppm (Figure 6), consistent with the proposed model. The two peaks at 77 and 143 ppm in this spectrum are due to an additional phase, LVP2.0, that can exist as a contaminant as described earlier in the XRD discussion (see above). Its characteristic NMR spectrum has been previously reported.[18] The sequence of $^7$Li MAS NMR spectra for various stages of delithiation starting with LVP3.0 (shown in Figure 7a) and culminating in LVP2.0 (Figure 7e) demonstrates that at the compositions $x = 2.75$ and $x = 2.25$, mixed phases (LVP 3.0/LVP2.5 and LVP2.5/LVP2.0) occur. These are evident in the intermediate spectra (Figure 7b,d). More importantly, it shows that the three single phases have unique and identifiable spectra (Figure 7a,c,e). Note that the LVP2.5 sample in Figure 7c is almost phase-pure, by comparison with the other sample in Figure 6.[22]

The five isotropic NMR peaks of LVP2.5 can be explained by the hyperfine (or Fermi-contact shift) interaction.[24] A "shift" of the $^{6,7}$Li NMR lines (compared to the reference at 0 ppm) arises from partial transfer of electron density from the $V^{n+}$ $t_{2g}$-like orbitals to the Li 2s orbital. For $n < 5$, it gives rise to a positive spin-density, and hence positive shift. This has been quantified to some degree in other materials such as $LiMn_2O_4$[25] and $LiMPO_4$ (M = Fe, Mn, Co, Ni).[26] The Fermi contact shift can also be a very sensitive probe of local bonding effects. In rhombohedral $Li_3Ti_2(PO_4)_3$, for example, it was shown that partial occupation of two sites (M3 and M′3) in the lattice led not to two, but multiple $^7$Li NMR signals (>7) due to the next-nearest-neighbor effect arising from the vacant and occupied sites surrounding those two sites.[27] Since the Fermi contact shift is dependent on the number of d-electrons and the nature of the orbital overlap-interaction, the Li−O−V bond lengths and bond angles determine the exact magnitude of the shift. Importantly, since here there is a 3:1 ratio of $V^{3+}(d^2)$ to $V^{4+}(d^1)$ we expect the two vanadium sites to give rise to different Fermi contact terms, and hence different isotropic shifts.

The precise ordering of the vanadium valence with respect to the Li sites makes the analysis more complex, however. Figure 8 shows the Li environments in one of the proposed space groups, $P\bar{1}$. The V(1) atom shown in cyan represents $V^{4+}$. V(1s), V(2), and V(2s) are shown in gray, indicating $V^{3+}$; the symbol "s" represents a pseudo-symmetric site as described above. In the case of Li(1) or Li(1s), there is only one possible contact shift, as these form a chain: $V(1s)^{3+}$−Li(1s)−$V(1)^{4+}$−Li(1)−$V(1s)^{3+}$. For Li(2), the vanadium atoms $V(1)^{4+}$, $V(2)^{3+}$, and $V(2s)^{3+}$ adjacent to it are different from the Li(2s) atom, where V(1s), V(2s), and V(2) are all 3+. This results in two different shifts for Li(2) and Li(2s). Similarly, $Li_3$ has contact with $V(1)^{4+}$, $V(2)^{3+}$, and $V(2s)^{3+}$. This is different from Li(3s), which is bonded to three 3+ cations, $V(1s)^{3+}$, $V(2)^{3+}$, and $V(2s)^{3+}$. There-

(24) Marichal, C.; Hirschinger, J.; Granger, P.; Ménétrier, M.; Rougier, A.; Delmas, C. *Inorg. Chem.* **1995**, *34*, 1773.
(25) Lee, Y. L.; Wang, F.; Grey, C. P. *J. Am. Chem. Soc.* **1998**, *120*, 12601.
(26) Tucker, M. C.; Doeff, M. M.; Richardson, T. J.; Finones, R.; Cairns, E. J.; Reimer, J. A. *J. Am. Chem. Soc.* **2002**, *124*, 3832.
(27) Aatiq, A.; Ménétrier, M.; Croguennec, L.; Suard, E.; Delmas, D. *J. Mater. Chem.* **2002**, *12*, 2971.

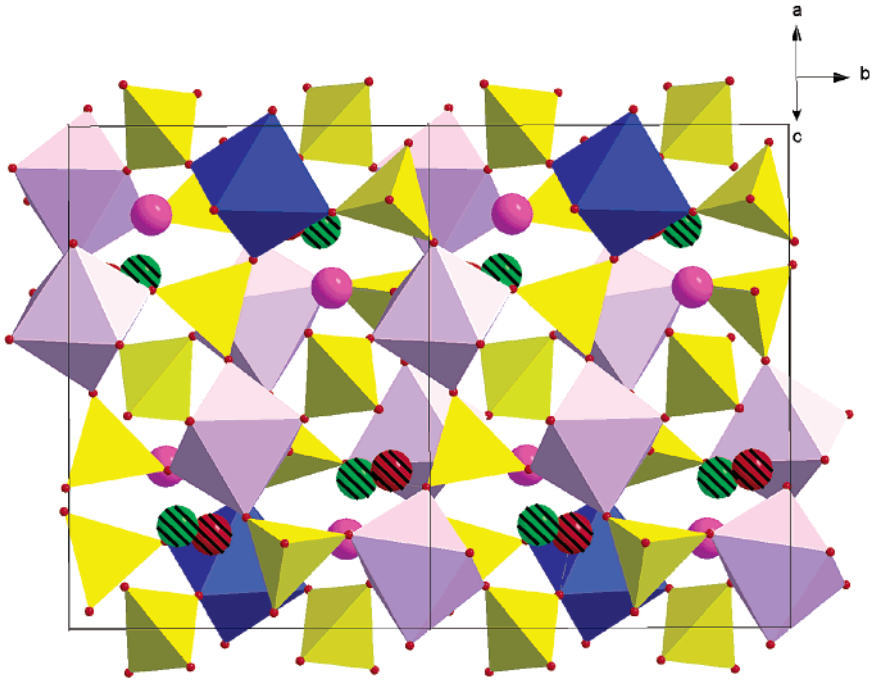


**Figure 5.** Proposed model of a $P\bar{1}$ cell showing long-range ordering of $V^{4+}$ (indigo) in the lattice.

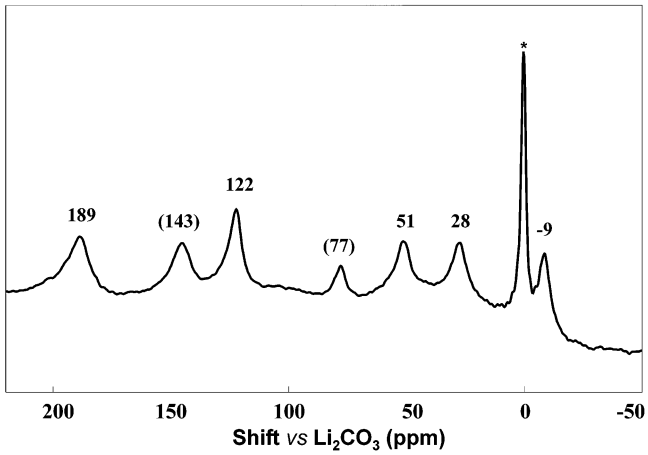


**Figure 6.** $^6$Li MAS NMR spectrum of $Li_{2.5}V_2(PO_4)_3$ showing the five isotropic chemical shifts (labeled, in ppm). The two lines arising from the second phase, $Li_{2.0}V_2(PO_4)_3$, are labeled with brackets; the peak marked with an asterisk corresponds to a small amount of residual Li salt on the surface of the crystallites.

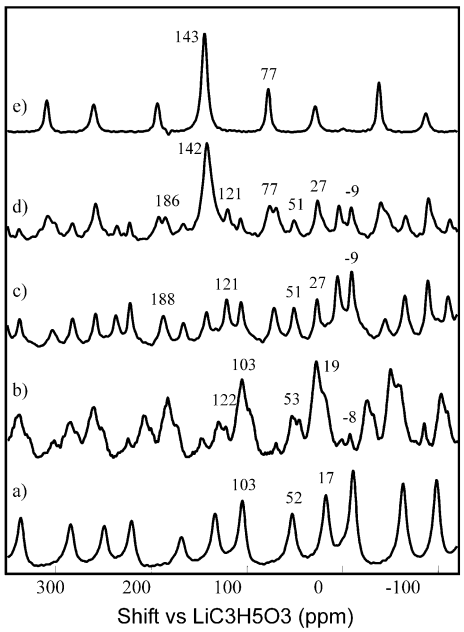


**Figure 7.** $^7$Li MAS NMR spectrum of $Li_xV_2(PO_4)_3$ on de-insertion from $x = 3 \rightarrow 2$. (a) $x = 3.0$; (b) $x = 2.75$; (c) $x = 2.5$; (d) $x = 2.25$; (e) $x = 2.0$. The isotropic chemical shifts in each spectrum are labeled (ppm).

fore, in total, five distinct contact shifts would result, consistent with the experimental NMR results. This could arise from either oxidation of V(1) or V(1s). We can rule out oxidation of V(2) or V(2s) since only four contact shifts would result in that case. Partial occupancy of the Li(2) and Li(3) sites may also have an influence on the area of the isotropic shifts, as shown by the integration results for the $^7$Li spectrum. The area percentages for the 188, 121, 51, 27, and −9 ppm peaks are 13.4, 20.2, 20.2, 19.5, and 26.7%, respectively. The exact assignment of these five shifts is difficult without DFT calculations. We note that consideration of the other two space groups (*Pc* and $P2_1$) also gives rise to five shifts by a similar argument, although the arrangement of the $V^{4+}$ in these lattices is slightly different.

**(2) Conductivity and Relationship to Other Phases.** The ac impedance spectra of $Li_xV_2(PO_4)_3$ phases are shown in Figure 9. All samples display a main pseudo-semicircle corresponding to the bulk ionic conduction of the materials, followed on the low-frequency side by an increasing branch (Warburg impedance). A second circle at intermediate frequencies, probably ascribable to intergrain impedance, is visible. On the high-frequency side (10 kHz), the intersection of the arc with $Z'$ provides an estimate of the electronic conductivity, on the order of $10^{-7}$ S/cm for all samples in accord with two-probe dc conductivity measurements. The extrapolation of the arc on the low-frequency side gives an estimate of the ionic conductivity (see Table 3). The value of $2.3 \times 10^{-8}$ S/cm at 300 K for

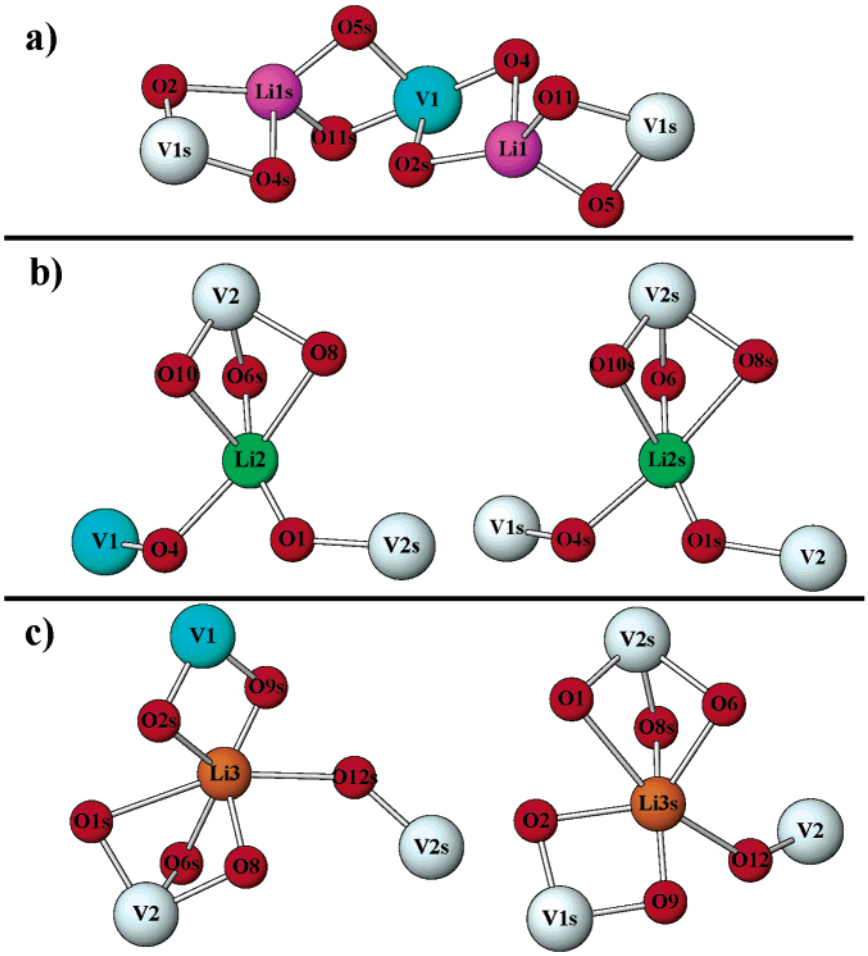


**Figure 8.** Five distinct environments for the three Li sites in $Li_{2.5}V_2(PO_4)_3$: (a) Li(1); (b) Li(2); (c) Li(3). $V^{4+}$ and $V^{3+}$ are shown in cyan and gray, respectively.

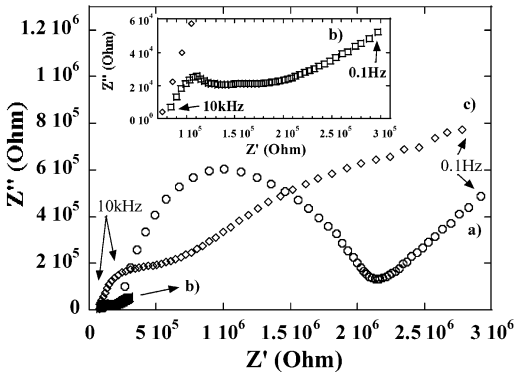


**Figure 9.** ac impedance spectra of $Li_xV_2(PO_4)_3$ in the frequency range from 10 kHz to 0.1 Hz at 300 KZ: (a) $x = 3.0$; (b) $x = 2.5$; (c) $x = 2.0$.

**Table 3. Electronic and Ionic Conductivity from ac Impedance Data for D-$Li_xV_2(PO_4)_3$ Phases**

| $x$ | thickness (mm) | $Z'$ (Ohm) high frequency | electronic conductivity | $Z'$ (Ohm) low frequency | ionic conductivity |
|---|---|---|---|---|---|
| 3 | 0.64 | $2.1 \times 10^5$ | $2.4 \times 10^{-7}$ | $2.2 \times 10^6$ | $2.3 \times 10^{-8}$ |
| 2.5 | 0.36 | $7.8 \times 10^4$ | $3.7 \times 10^{-7}$ | $1.5 \times 10^5$ | $1.9 \times 10^{-7}$ |
| 2 | 0.40 | $7.2 \times 10^4$ | $4.4 \times 10^{-7}$ | $7.4 \times 10^5$ | $4.3 \times 10^{-8}$ |
| 1 | 0.20 | $8.0 \times 10^4$ | $2.0 \times 10^{-7}$ | $1.6 \times 10^6$ | $9.7 \times 10^{-9}$ |
| 0 | 0.20 | $1.1 \times 10^5$ | $1.4 \times 10^{-7}$ | | |

the pristine material, $Li_3V_2(PO_4)_3$, is in accord with previous measurements that reported values of about $1 \times 10^{-8}$ S/cm. [15]

The behavior of $Li_{2.5}V_2(PO_4)_3$, however, is unique. It possesses the highest ionic conductivity (more than an order of magnitude) by comparison to the fully lithiated phase. This can be explained by the partial vacancy distribution on the Li(2) and Li(3) sites, a property that is shared by the other members of the fast-ion conductors in this family. This includes the well-known superionic material $\gamma$-$Li_3Sc_2(PO_4)_3$, whose lithium ion occupation is compared to that of pseudo-orthorhombic $Li_{2.5}V_2(PO4)_3$ in Scheme 1. Both lattices share similar lithium site populations, namely, full occupancy of Li(1) and partial occupancy of Li(2) and Li(3). In the scandium framework, this disorder over the two lithium sites leads to enhanced mobility. Comparison of the conductivities of LPV2.5 and the $\gamma$- scandium phase is difficult since the latter is stable only at high temperatures and reverts to the α-phase on cooling to ambient temperature. For the vanadium compound, it has been proposed that the phase transition to the $\gamma$-analogue occurs above 180 °C. A room-temperature variant of $\gamma$-$Li_3V_2(PO_4)_3$ has been reported, however, which is stabilized by the addition of a 4+ cation to the α-lattice, to give $Li_{3-x}(V_{1-x}Zr_x)_2(PO_4)_3$.[15] Its reported structure based on refinement of neutron data shows that all three lithium sites have partial vacancies. This gives rise to a much lower activation energy for ion conduction than in the pristine α-phase (i.e., similar to the scandium $\gamma$-phase) and a conductivity between $3 \times 10^{-7}$ and $1 \times 10^{-6}$ S/cm, depending on the degree of substitution, $x$. The ionic

**Scheme 1. Lithium Ion Location at $z \approx {}^1/_4$ in (A) $Li_{2.5}V_2(PO_4)_3$ and (B) $\gamma$-$Li_3Sc_2(PO_4)_3$[a]**

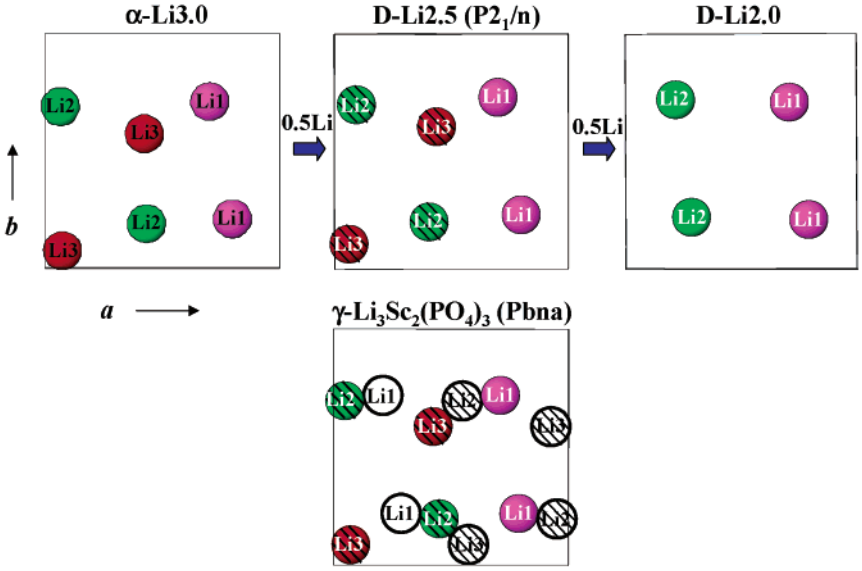


[a] The sites for the *Pbna* cell ($\gamma$-phase) are "doubled" in the cell due to the orthorhombic symmetry, and hence the equivalent symmetry sites in the *Pbna* phase are indicated with open white circles for this lattice to make the comparison with the monoclinic cells clear.

conductivity of LVP2.5, $1.9 \times 10^{-7}$ S/cm, is very close to these values. The similarity is even closer than the numbers imply, since the measurements on the Zr-stabilized phase were performed on pellets sintered at 1100 °C, whereas ours were carried out on room-temperature pressed pellets.

For the phases with lithium content lower than LVP2.5, Table 3 shows that the ionic conductivities decrease with the lithium content. This is expected since $\sigma = ne\mu$ (where $n$ is the number of conducting species and $\mu$ is the mobility). That is, it is partly due to decreased carrier concentration, which is especially true for $LiV_2(PO_4)_3$. A substantial conductivity difference is not expected for LVP2.5 vs LVP2.0, however. We attribute the lower conductivity in LVP2.0 to its highly ordered lithium distribution, as described in our previous report. Both and its pseudo-symmetry site are fully occupied in this lattice, and therefore ion hopping would have to occur via population of a more energetically unfavorable site.

## Summary and Conclusions

We have used combined diffraction and spectroscopic methods to determine the structure of an intermediate phase corresponding to a distinctive feature in the electrochemical charge curve of $Li_3V_2(PO_4)_3$. Formation of $Li_{2.5}V_2(PO_4)_3$ is signaled by a small voltage jump on lithium extraction during oxidation. However, it can also be readily prepared by stoichiometric chemical oxidation of the starting phase. Our structural studies using X-ray and neutron powder diffraction show that it adopts almost pseudo-orthorhombic structure (formally monoclinic in the $P2_1/n$ space group, but with a $\beta$ angle very close to 90°) that is related to its high-temperature fast-ion conducting analogue, orthorhombic $\gamma$-$Li_3V_2(PO_4)_3$. The similarity can be explained more fully by noting that three sites in the orthorhombic $\gamma$-phase are split into six lithium sites (Li(1)/Li(1s), Li(2)/Li(2s), Li(3)/Li(3s)) in the monoclinic α-phase by the reduction in symmetry. In the latter, only one of each pair (Li1, Li2, and Li3) are fully occupied, leaving the others empty. However, in the $\gamma$-$Li_3Sc_2(PO_4)_3$ phase, Li(1) is fully occupied, but two lithium ions are disordered over the Li(2) and Li(3) sites.[28] In $Li_{2.5}V_2(PO_4)_3$, Li(1) is also fully occupied, and 1.5 lithium are disordered over the two Li(2) and Li(3) sites. Hence, one identical lithium site is fully occupied in both cases, and disorder combined with partial site occupancy over the remaining sites leads to enhanced lithium ion mobility. This gives rise to ionic conductivity in $Li_{2.5}V_2(PO_4)_3$ of more than an order of magnitude greater than that of the neighboring phases in the composition diagram ($x = 3.0; 2.0$).

The localization and apparent short-range ordering of the $V^{4+}$ in the framework revealed by NMR spectroscopy gives rise to five independent Li sites that can be distinguished on the basis of their interaction with the $V^{3+}$ and $V^{4+}$ in the lattice. Evidence of long-range ordering of the $V^{4+}$ was not suggested by careful fitting of the diffraction data to any subcell that would account for such order. Since there are different ways to arrange the $V^{4+}$ in the lattice, such a cell would probably not be unique, and hence long-range ordering may be disrupted. It is interesting to note that the disorder in the lattice *vis-a-vis* both electron and lithium location is in sharp contrast to the related $Li_2V_2(PO_4)_3$ phase, where lithium ordering in the lattice is correlated to long-range $V^{4+}$ ordering—and hence to a pinning of the charge carriers.

**Acknowledgment.** We thank the Institut Laue-Langevin, Grenoble, France, and E. Suard (ILL) for her able assistance. We are grateful to W. P. Power (Waterloo) and M. Anne (CNRS, Grenoble) for helpful discussions. S.C.Y. thanks Prof. Mark Pritzker for use of the ac impedance instrument and Dr. Robert Reed for help

(28) The site population of the high-temperature $\gamma$-$Li_3V_2(PO_4)_3$ phase has not yet been crystallographically determined, but it is assumed to be identical to the high-temperature $\gamma$-scandium phase, $Li_3Sc_2(PO_4)_3$ (see ref 15).

with the EPR experiments. L.F.N. acknowledges NSERC for funding the research program and the CNRS (Grenoble) for a visiting professorship and is grateful to the Canada-France Foundation for providing travel funds. We are saddened by the loss of our valued co-author, Hiltrud Grondey.

**Supporting Information Available:** Summary of the structure refinement, bond lengths, and selected angles were reported in the tables for D-$Li_{2.5}V_2(PO_4)_3$ (PDF and CIF). This material is free of charge via the Internet at http://pubs.acs.org.

CM034802F